Proceedings of ASME Turbo Expo 2024
Turbomachinery Technical Conference and Exposition
GT2024
June 24-28, 2024, London, United Kingdom

GT2024-121397

EVALUATING THE ENERGY RECOVERY POTENTIAL IN INDUSTRIAL GAS PIPELINE NETWORKS: A PRELIMINARY ANALYSIS OF GAS EXPANDER APPLICATIONS FOR NITROGEN, OXYGEN AND HYDROGEN

Mattia Baiguini
University School of Advanced Studies
Pavia, Italy

Michele Doninelli
University of Brescia
Brescia, Italy

Gioele Di Marcoberardino
University of Brescia
Brescia, Italy

Paolo Giulio Iora
University of Brescia
Brescia, Italy

Costante Mario Invernizzi
University of Brescia
Brescia, Italy

ABSTRACT

The aim of this work is to analyse the potential electrical energy that can be produced from the installation of expanders in the gas pressure reducing stations of industrial gases networks (oxygen, nitrogen and hydrogen). This solution is well established in natural gas grid but not yet implemented in existing technical gases networks. In the first part, the theoretical energy recovery potential is investigated by calculating the isentropic expansion specific power under different expander inlet temperatures and pressure ratios. Then the evaluation of adopting radial or axial expander is considered according to typical operating conditions: in particular, the design of axial expander is carried out with an open-source code. Eventually the design and the impact of the gas expanders solution is evaluated in selected industrial processes for each investigated technical gas. A discussion on practical issues is proposed. Radial expander could reach an isentropic efficiency of 89% while efficiency of 94% is obtained with an axial configuration with compact machinery. The application of gas expander in possible scenarios leads to annual energy production up to 19 GWh (O_2 expander in blast furnace) with an utilization factor of 90% and cost of production ranges from 16 to 37 $/MWh with an avoided emission up to 1062 $tCO_{2,eq}/y$. Results show an interesting potential for the proposed solution: however, the application strongly depends on adequate gas flow rate and operating pressure with a niche market now.

Keywords: Power generation, Expansion recovery, Turbomachines, Axial turbine

NOMENCLATURE

Acronyms

CAPEX	Capital expensive, $
CEPCI	Chemical Engineering Plant Cost Index
EE	Electric energy, kW/h
EIGA	European Industrial Gases Association
EIT	Expander Inlet Temperature, °C
EOT	Expander Outlet Temperature, °C
GE	Gas Expander
LCOE	Levelized Cost of Electricity, $/MWh
NG	Natural Gas
OPEX	Operative expansive, $/y
POD	Point Of Delivery
POU	Point of Utilization
SP	Size Parameter, m

Roman and Greek letter

C	Equipment cost, $
$E_{CO_2,eq}$	Avoided emission, $t_{CO2,eq}/y$
M	Mach number, -
MM	Molar weight, kg/kmol
P	Pressure, bar
R	Universal Gas Constant, 8.314 kJ/kmolK
V	Volumetric flow rate, m^3/s
V_r	Expansion volumetric ratio, -
$\dot{W}$	Power, kW
$e_{CO_2,eq}$	Specific emission, $kg_{CO2,eq}/MWh$
$\dot{m}$	Mass flow rate, kg/s
n_{st}	Number of stages, -
u	Peripherical speed, m/s

Δh	Specific power, kJ/kg
Λ	Degree of reaction, -
β	Pressure ratio, -
γ	Specific heat ratio, -
η	Efficiency, -
λ	Hub-to-tip ratio, -

Subscription

g	Generator
in	Inlet
is	Isentropic
mix	Electric generation mix
out	Outlet
pol	Polytropic
rel	Relative

1. INTRODUCTION

In the context of energy recovery, replacing a pressure reduction valve in natural gas (NG) systems with a gas expander (GE) offers a consistent solution for harnessing energy from high gas flow rates at medium-high pressure. This approach has been extensively studied in the literature and numerous turbomachinery companies now offer this technology[1]. The GE boasts a less complex design and construction compared to conventional power cycles and it integrates easily with existing natural gas distribution networks [1]. Moreover, this concept can be extended to pipeline networks used for distributing and transporting industrial gases such as hydrogen (H_2), oxygen (O_2), and nitrogen (N_2) (Table 1). Since the supply of these gases to various industry sectors is typically constant and well-programmed, the machinery isn't subjected to the fluctuations common in natural gas network systems [2].

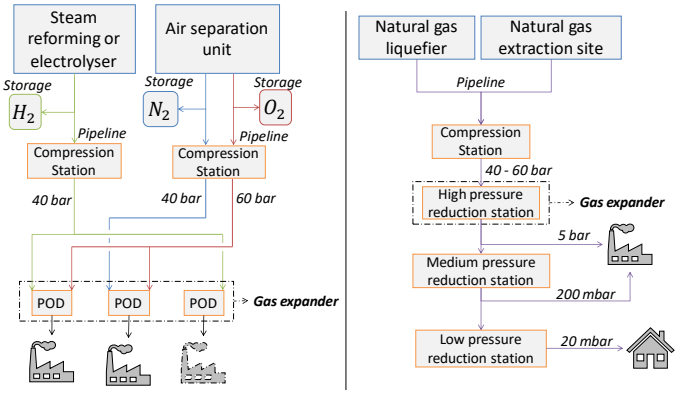

FIGURE 1: INDUSTRIAL GASES (LEFT) AND NATURAL GAS (RIGHT) DISTRIBUTION NETWORK.

As shown in Figure 1 – left, after the production phase, the mentioned gases can either be stored at high pressure, liquefied or sent to the compression station for dispatch to the point of delivery (POD), where they are expanded to the desired pressure before being utilized in the specific industrial process at the point of utilization (POU). Typically, the delivery pressure up to 40 bar for H_2 and N_2 and up to 60 bar for O_2 [3]. This network features a simpler architecture compared to the natural gas (NG) network (Figure 1 - right), as only one reduction station is employed.

Oxygen is well known as a gas implemented in the steel industry for the casting process and other treatments, moreover O_2 finds application in the glass, cement, paper industries and in the wastewater treatment. On the contrary, nitrogen is well established as an inert gas in chemical and food manufacturing and cooling medium in glass production. Besides being a potential energy carrier, H_2 finds applications in chemicals, food and steal industry.

TABLE 1: PROPERTIES OF THE INVESTIGATED INDUSTRIAL GASES IN COMPARISON WITH NATURAL GAS (ASSUMED 100% METHANE). DATA FROM NIST DATABASE.

Properties	H_2	O_2	N_2	NG
Molecular weight (MM)	2.01	31.99	28.01	16.04
Boiling point at ambient pressure, °C	-253	-183	-195	-161
Density at 25°C and 50 bar, kg/m^3	3.94	66.44	56.73	35.26
Specific heat capacity at 25°C and 50 bar, kJ/kgK	14.43	1.0013	1.12	2.57

According to the European Industrial Gases Association (EIGA) [4], the global industrial gases market reached a size of €91 billion in 2022, with the USA, EU27, and China collectively accounting for 65% of the global gas market share. In Europe, the market has experienced growth of 4.4% over the decade spanning from 2012 to 2022, reaching a value of €18 billion. The primary traded gases in Europe are O_2 (32%), N_2 (23%), and H_2 (13%) [4]. Additionally, EIGA reports that the main consumers of industrial gases are the chemicals, manufacturing, and metallurgy industries, with gases supplied 40% via cylinders, 26% via bulk deliveries, and 32% through pipeline or onsite production.

As example the company SIAD Macchine e Impianti produces Air Separation Unit (ASU) with a capacity up to 90 kNm^3/h for O_2 and 270 kNm^3/h for N_2 [3], while the Linde Engineering company realizes ASU of a capacity up to 150 kNm^3/h for O_2 and 340 kNm^3/h for N_2 [5]. Meanwhile H_2 can be produced or from methane steam reforming with a capacity up to 12 kNm^3/h [6] or from electrolysis where the output is strongly depend on the size of the stack. As well, the European Hydrogen Backbone Initiative highlights that, in the energy transition, an H_2 pipeline distribution network should be implemented, estimating an overall length network of 57600 km by 2040 linking all the EU state members [7]. Examples of industrial gas expanders in literature are limited. Kong et al. [8] introduced a nitrogen GE, which utilizes the pressure reduction process from the pipeline. GE are also utilized in liquefaction processes. In ASU, following

[1] Turboden, Atlas Copco, Backer Hughes and Cryostar.

the main heat exchanger, air undergoes expansion from 5.9 to 1.3 bar to achieve a temperature of approximately -185°C, with the assistance by an expander [9] [10]. Similarly, in the NG liquefaction process, cryogenic temperatures (-133°C for N_2) are attained using a nitrogen chiller, with energy recovery facilitated by the adoption of a GE [11]. For the sake of the discussion, it is worth to mention few examples of such infrastructure with particular attention to the northern Italian region. The ASU production site of SIAD, located in Bergamo, supplies N_2 to few surrounding chemical manufacturing industries and a biogas from waste production site where O_2 is supplied too[2]. Regarding steel industry, from the same ASU site, O_2 is sent to a foundry located in the city of Brescia area[3]. An Air Liquide production site, located in the metropolitan area of Milan, deliveries oxygen steel industries[4] and glass one[5]. Moreover, the same plant supplies N_2 to a petroleum refinery located 80 km southwest of Milan[6]. Air Liquide operates other oxygen pipelines, including, as an example, Scotford (1000 tonnes/day), Hamilton (2700 tonnes/day), Quebec (20 km pipeline), and the us gulf coast (16000 tonnes/day) [12]. Praxair, in collaboration with Air Liquide, manages a 500 km pipeline system in Europe's Rhine-Ruhr area [12]. Linde, present in Europe and expanding networks in China, offers additional opportunities for oxygen transportation arrangements [12]. An other example of pipeline network is reported by Vinson in [10], where 3 ASU plant from air products company serve almost 50 customers in an industrial area in the USA.

The aim of this work is to present various aspects of the innovative concept of GE for industrial gases. Following a literature review, a preliminary analysis is conducted to estimate the isentropic efficiency of the expander, considering both radial and axial designs. For the latter, a mean-line analysis is performed using a MATLAB open-source code to assess not only performance but also geometry and velocities under different conditions. Subsequently, four case studies are presented, evaluating energy production, cost, and emissions reduction. Finally, a discussion on practical issues, such as safety and material compatibility, is undertaken.

2. METHODOLOGY

A scheme of the GE plant is presented in FIGURE 2. The GE comprises several components, including a distribution valve and a reduction one for safety precaution, the actual turbomachinery, an electric generator, and optionally, a heat exchanger. The addition of a heat exchanger depends on whether the industrial process offers a low to medium waste heat source that can be utilized to elevate the inlet temperature of the GE.

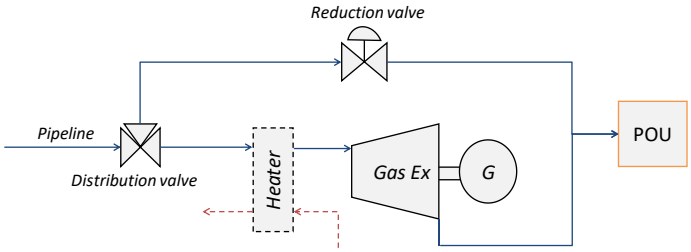

FIGURE 2: INDUSTRIAL GAS EXPANDER SCHEME

2.1 Gas expander assessment

A preliminary assessment of the potential of the gas expander is carried out estimating the isentropic specific power (w_{is}) produced by the expansion of the different gases as a function of the pressure ratio ($\beta = P_{in}/P_{out}$) ranges from 2 to 20 (N_2 and H_2) or 30 (O_2 only). Three expander inlet temperatures (EIT) are considered based on the potential for preheating the gas using different levels of low-grade heat recovery available in the industries (25°C, 50°C, and 100°C). This aligns with the substantial amount of waste heat potential (300 TWh/year) in Europe, one-third of which is available at temperatures below 200°C [13]. The software Aspen Plus V14 [14] is used with the REFPROP V10 [15] database for the calculation of the thermodynamic properties. As a second step, the isentropic efficiency (η_{is}) for radial and axial configurations expanders is evaluated considering a mass flow rate ($\dot{m}$) from 5 to 35 kg/s, reflecting the standard production scale of a centralized air separation unit or steam reformer [3] [5] [6]. Concerning the radial configuration, the performance map presented in the work of Perdichizzi and Lozza [16] serves as a reference. The isentropic efficiency (η_{is}), at the optimum specific rotational speed, is function of volumetric expansion ratio ($V_{r,is}$) and the size parameter (SP) which are defined as follows (Eq. (1) and (2)):

$$V_{r,is} = \frac{V_{out,is}}{V_{in}} \tag{1}$$

$$SP = \frac{\sqrt{V_{out,is}}}{w_{is}^{0.25}} \tag{2}$$

$$w_{is} = \left(\frac{\gamma}{\gamma-1}\right)\frac{R}{MM}\,EIT\left(1-\beta^{-\left(\frac{\gamma}{\gamma-1}\right)}\right) \tag{3}$$

Where V is the volumetric flow rate and w_{is} is the isentropic specific power, that for ideal case can be express as Eq. (3). R and MM are the gas universal constat and the molecular weight, while, assuming ideal gas behaviour, γ is the specific heat is equal to 1.4 for all the analysed gases [17]. For axial turbine, η_{is} is evaluated with Eq. (5) by calculating the polytropic efficiency η_{pol} according to the correlation in Eq. (4) proposed in [17].

[2] Relate information: i) N_2 pipeline SIAD - Bidachem, ii) N_2 pipeline SIAD - Corteva and iii) Map of N_2 and O_2 pipelines to Montello S.p.A

[3] Relate information: O_2 pipeline SIAD – Fonderie Torbole.

[4] Relate information: O_2 pipelines Air Liquide – ORI Martin and Air Liquide – Alfa Acciai.

[5] Relate information: O_2 pipeline Air Liquide – Vetrobalsamo

[6] Relate information : N_2 pipeline Air Liquide – ENI

$$\eta_{pol} = 0.94(1 - 0.02668 \log^2(SP)) \quad (4)$$

$$\eta_{is} = \frac{1 - \beta^{-\frac{\gamma-1}{\gamma}\eta_P}}{1 - \beta^{-\frac{\gamma-1}{\gamma}}} \quad (5)$$

After this initial assessment, the analysis focuses on designing an axial expander using the open-source code AxialOpt: a MATLAB tool for the mean-line design optimization of axial turbines [18]. The machinery is evaluated considering an EIT of 50°C, consistent with the value used for NG gas expanders [19], at various pressure ratios, mass flow rates and numbers of stages. Additionally, the one-dimensional design of a diffuser is taken into account to recover part of the kinetic energy at the exit of the last rotor. The Kacker-Okapuu model [18] is chosen to calculate the aerodynamic losses in axial turbomachinery. A free vortex distribution model is employed to avoid non-negative degrees of reaction at the hub [17]. The main parameters for the assessment analysis are outlined in TABLE 2 and are sourced from Lozza et al. [20], while a more detailed description of the code can be found in [18].

TABLE 2: PARAMETERS AND CONSTRAINS OF THE AXIAL EXPANDER DESIGN ANALYSIS

Parameter	Value
EIT	50°C
Expansion ratio	3-5-10
Mass flow rate	5-10-20-35 kg/s
Number of stages	1-2-3
Hub-to-tip ratio	$\lambda > 0.8$
Blade height mean diameter ratio	$0.01 < h/D_m < 0.25$
Hub degree of reaction	$\Lambda > 0$
Relative Mach number at rotor inlet	$M_{rel,in} < 0.8$
Relative Mach number at rotor outlet	$M_{rel,out} < 1.4$
Blade tip peripheral speed	$u_{tip} < 400$ m/s

2.2 Case studies and economic analysis

Few case studies (Table 3) have been selected to provide a more comprehensive understanding of the technology potential. For the implementation of O_2 GE, three cases have been selected. *Case 1* refers to an oxygen blast furnace as presented by Arasto et al [22], while *Case 2* considers oxy-fuel combustion in two glass melting furnaces industry for bottle production [23]. *Case 3* also originates from the same industry of *Case 2*, where the O_2 is received from the nearby Air Liquide ASU site at 30 bar (see note 5). In the ASU plant, the gas is compressed in liquid phase at 60 bar and then evaporated at ambient temperature. A fraction of O_2 is directly delivered to a high-pressure pipeline (see note 4), while another fraction is reduced to 30 bar and sent to mentioned industry. The application of H_2 and N_2 GEs can also be found in the glass industry (*Case 4*), where flat glass is produced in an inert atmosphere of H_2 and N_2 ($90\%_{vol}$ N_2): the two gases are mixed and sent to the process at a pressure of around 3-6 bar [21].

TABLE 3: DATA FOR THE CASE STUDIES

	Case	Gas	P_{in} [bar]	P_{out} [bar]	Flow [kg/s]
1	Blast furnace	O_2	60(b)	6(a)	23.9(a)
2	Glass melting furnace	O_2	30(a)	3(a)	13(c)
3	Pressure reduction in ASU production	O_2	60(a)	30(a)	13(c)
4	Inert atmosphere in tin bath	N_2	40(b)	4(a)	0.7(a)
		H_2	40(b)	4(a)	0.16(a)

(a) Data from publications or reports. (b) assumed data. (c) calculated data from available info.

Data for all investigated cases are reported in [21]; some are calculated from actual available data (e.g., *Case 4* considers a production of 600 tonnes/day of float glass), while others are assumed considering a pipeline delivery system. Following the scheme in Figure 2, the presence of a heat exchanger providing the necessary heat for increasing the gas temperature is anticipated in the mentioned high-temperature process industries. Therefore, the EIT is selected as 50°C, except for *Case 3*, while the gas from the pipeline is assumed to be at 15°C. In *Case 3*, heat recovery is quite challenging: the air entering the ASU is intercooler compressed, and the water used as coolant does not undergo significant temperature increase [9], hence an EIT of 25°C is assumed.

The investigation begins with assessing the feasibility of adopting either radial or axial expanders, followed by an analysis consistent with the presented methodology. Subsequently, the study proceeds to calculate the annual electrical energy production, estimate the avoided emissions and determine the Levelized Cost of Electricity (LCOE). The annual electrical energy production (EE) and the avoided emissions ($E_{CO_2,eq}$) are computed as follows in Eq. (6) and (8):

$$EE = 8760 UF \cdot \dot{W} \quad (6)$$

$$\dot{W} = \eta_g \eta_{is} (\dot{m} w_{is}) \quad (7)$$

$$E_{CO_2,eq} = \frac{EE}{\eta_{mix}} e_{CO_2,eq} \quad (8)$$

Where UF is the utilization factor equal to 90%, while $\dot{W}$ in Eq. (7) is the electric power generated from the GE. η_g, equal to 96%, is the efficiency of generator and gearbox (necessary to match the electric grid frequency). The ratio varies from 1.5 to 200 depending on type of gear and it is possible to obtain significant performance even with elevated ratio [24]. $e_{CO_2,eq}$ is referring to the average European emission for power generation equal to 250 $kg_{CO2,eq}$/MWh [25], while η_{mix} is the average electric generation efficiency for the European mix and it is assumed equal to 45%.

For the initial estimation of the LCOE, equipment cost assumptions are derived from [26][27] (Table 4), while operation and maintenance (OPEX) assumptions are based on [28]. The

cost data in [26] (for the expander only) and [27] are related to power cycle components retrofitted, as determined by an extensive review. These data serve as a suitable basis for preliminary assessment. For specific formula coefficients, please refer to [26] and [27]. The LCOE is calculate according to the Eq. (9):

$$LCOE = \frac{CAPEX_{2023} \cdot CRF + OPEX_{2023}}{EE} \quad (9)$$

The cost correlations are presented in Table 4: UA in kW/K, $\dot{W}$ in MW in expander correlation and kW in generator one. The term n_{st} is the stages number, while a is a pressure-dependent factor. The UA is computed considering a counter current heat exchanger where the temperatures of the hot side are 80°C (inlet) and 25°C (outlet).

TABLE 4: COST CORRELATIONS. 2014 DATA.

Component	Cost correlation
Heat Exchanger	$C = C_0 \left(\frac{UA}{UA_0}\right)^{0.9} a$
Expander	$C = C_1(\dot{W})^{0.99} + C_2 \left(\frac{SP}{SP_0}\right)^{1.06} n_{st}^{1.18}$
Generator	$C = C_0 \left(\frac{\dot{W}}{\dot{W}_0}\right)^{0.67}$
Gearbox	40% of generator cost

The equipment costs are actualized by using the Chemical Engineering Plant Cost (CEPCI) index as reported in TABLE 5 [29]. The capital expensive (CAPEX) are the sum of the equipment total cost and cost of balance of plant. For the economic analysis, a capital recovery factor (CRF) of 6.4% has been used in Eq. (9), considering a lifetime of 25 years and an interest rate of 4%.

TABLE 5: DATA FOR THE LCOE ANALYSIS

Parameter	Value
Cost equipment	$C_{2023} = C_{2014} \left(\frac{CEPCI_{2023}}{CEPCI_{2014}}\right)$
Balance of plant	40% of equipment total cost
Specific OPEX	0.01 $/kWh
Gas temperatures[(a)]	15°C (from pipe) / 50°C (EIT)
Hot side heat exchanger[(b)]	80°C (inlet) / 25°C (outlet)
CRF	6.4%
CEPCI 2023/2014	798.7 / 567.5

(a) For *Case 4* EIT = 25°C. (b) No heat exchanger in *Case 4.*

3. RESULTS

3.1 Gas expander potential energy recovery

Figure 3 and Figure 4 illustrates the ideal specific power produced by the GE at various operating conditions for the three investigated industrial gases. Generally, an increase in the EIT and the pressure ratio positively impacts the specific work. However, differences in results among the gases depend on their thermophysical properties. Despite oxygen and nitrogen having different inlet pressures (60 bar for O_2 and 40 bar for N_2), they exhibit similar outcomes. Examining the ideal specific power expressed in Eq. (3), the lower MM of the N_2 results in higher values at the same pressure ratio. Specifically, the O_2 GE can achieve an ideal specific work of 206.6 kJ/kg, while the N_2 GE reaches a maximum work of 221.1 kJ/kg. These closely aligned values stem from the fact that, in the ideal case, w_{is} depends on the pressure ratio and the molar weight [17]. On one hand, an increase in P_{in} raises the β at equal P_{out}, favoring the O_2 expander. On the other hand, a lower molar mass corresponds to higher specific work, benefiting N_2 (see Table 1). Thanks to the lowest MM, the H_2 GE (Figure 4) shows the highest specific work even at low pressure ratio, reaching value up to 3100 kJ/kg.

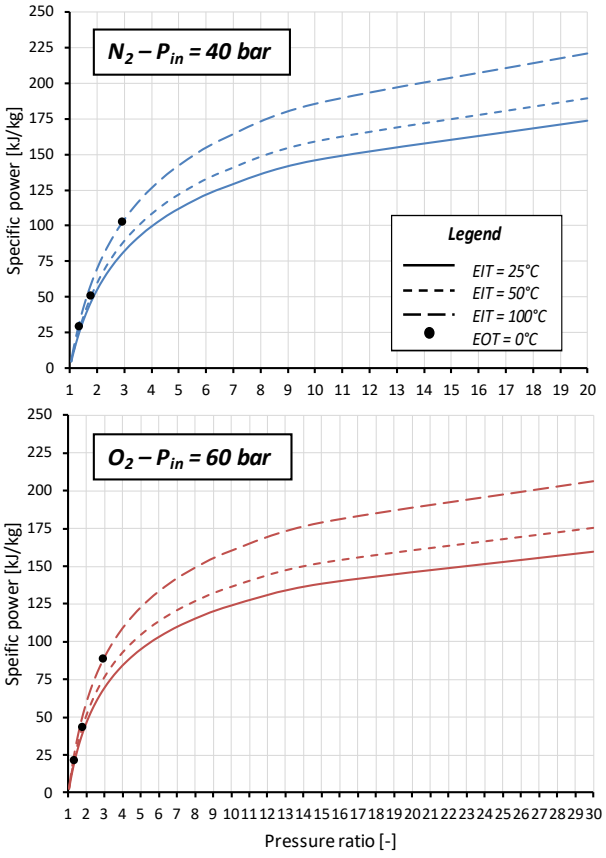

FIGURE 3: IDEAL SPECIFIC WORK FOR NITROGEN AND OXYGEN. P_{IN} = 40 BAR AND P_{IN}=60 BAR FOR O_2. DOT POINTS REFER TO THE CONDITIONS WHERE THE EXPANSION OCCURS BELOW 0°C.

Considering the expander outlet temperature (EOT), a value below 0°C is obtained already a low β between 1.3 and 3 for all the investigated gases because the heat capacity ratio does not significantly change. That leads to the conclusion that for a wide range of pressure ratio, the EOT is always below 0°C and EOT

reaches values in the range of -115 and -160°C, exploiting the maximum pressure ratio possible.
As final comparison, typically a NG GE (assuming 100% methane) is employed in the high to medium pressure station and has a P_{in} equal to 50 bar and it is expanded until P_{out} of 5 bar. That leads to an isentropic specific work that varies from 265 to 360 kJ/kg depending on EIT (from 25°C to 100°C) reaching a maximum value of 420 kJ/kg at EIT equal to 100°C and β equal to 25. Meanwhile a EOT below 0°C is obtained at β of 1.4, 2.05 and 3.6 at EIT equal to 25, 50 and 100°C respectively.

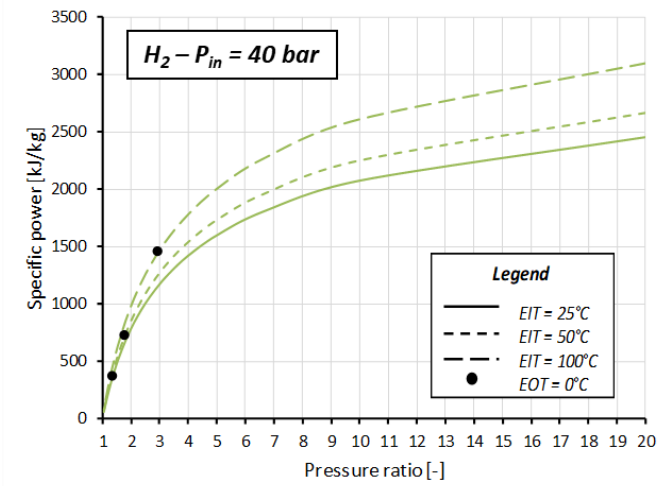

FIGURE 4: IDEAL SPECIFIC WORK FOR HYDROGEN. DOT POINTS REFER TO THE CONDITIONS WHERE THE EXPANSION OCCURS BELOW 0°C.

3.2 Preliminary analysis on radial and axial expander

Figure 5 illustrates the isentropic efficiency of the turbomachinery in both radial and axial configurations. As a general rule, the efficiency of a radial expander tends to be lower than that of an axial one due to higher aerodynamic and friction losses, as well as secondary flow effects that penalize the overall performance of the machine [17].
In terms of radial design, the resulting efficiency varies from 86% to 89%. It is noteworthy that the map presented by Perdichizzi and Lozza [16] indicates a rapid change in efficiency for SP values ranging from 0.01 to 0.04 m and $V_{r,is}$ up to 9. The trend of the iso-efficiency line suggests that operating conditions where SP is above 0.04 m exhibit limited variation in η_{is}, and it is possible to achieve isentropic efficiency higher than 86% while maintaining modest $V_{r,is}$. The authors attribute this phenomenon mostly to the stator's extremely short blade height and the extremely low volume flow rate at the rotor inlet compared to that at the rotor exit. The isentropic outlet volumetric flow for N_2 and O_2 ranges from 0.6 to 2.15 m^3/s (depending on $V_{r,is}$), while the radial GE for H_2 achieves an efficiency in the range of 88-89%, even with a small mass flow. In fact, the isentropic outlet volumetric flow ranges from 2.11 to 4.91 m^3/s, and the w_{is} is one order of magnitude higher. Due to the imposed boundary conditions, all gases exhibit almost the same $V_{r,is}$. For a pressure ratio of 3, $V_{r,is}$ is equal to 2.1, while at a pressure ratio of 10, $V_{r,is}$ is 5. On the other hand, the SP increases with the increase in w_{is} and mass flow rate, indicating that H_2 GE and high mass flow rate GEs exhibit the best performance within the family of radial expanders. The O_2 GE with a β value of 10 and $\dot{m}$ of 5 kg/s achieves the lowest efficiency (approximately 86%), while an η_{is} of 89% is achieved for H_2 at a β value of 3 and a mass flow rate of 35 kg/s.
Moving to axial gas expander, the correlation in Eq. (4) expresses the polytropic efficiency considering the size of the turbomachinery. The efficiency ranges from 89% to almost 95% depending on SP and β. As the value of SP increases, the efficiency increases accordingly due to the minor efficiency losses presented in larger machinery. Axial GEs for N_2 and O_2 exhibit efficiency ranging from 89.5% to 94%, while H_2 machineries are characterized by efficiency ranging from 91.5% to 94.8%.

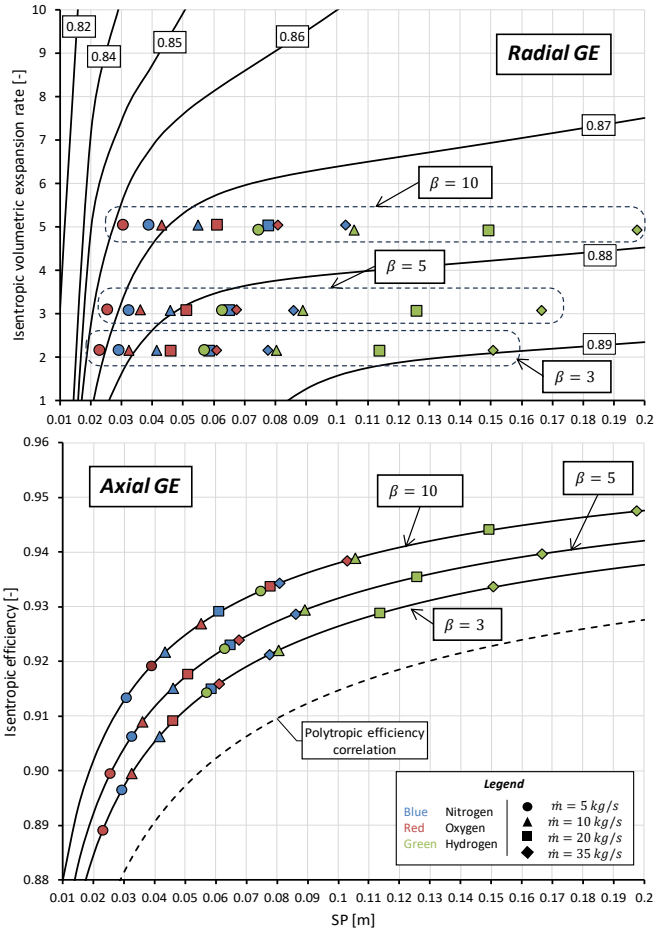

FIGURE 5: PRELIMINARY ISENTROPIC EFFICIENCIES FOR THE GAS EXPANDER IN RADIAL (UPPER) AND AXIAL (LOWER) CONFIGURATION. LABELS CORRESPOND TO ISO EFICIENCY LINES.

Under the same conditions, the adoption of an axial expander generally results in a performance increase of 2% in small

turbomachinery and 5% in larger ones. The recovered shaft power varies widely, ranging from 250 kW to 5 MW for O_2 and N_2 gas expanders, while for hydrogen, the range shifts to 5 MW to 75 MW. This preliminary analysis indicates that achieving large outputs requires high-consumption industries such as steel mills; however, even small consumers can benefit from gas expanders. Nonetheless, a detailed design of the turbomachinery is necessary to identify critical issues and actual performance.

3.3 Design of an axial expander

For the analysis, the code AxialOpt has been used to extrapolate not only the isentropic efficiency but also other conventional quantities for turbine such as the velocity triangles, blade profiles, chassis dimensions and the thermodynamic results from each stage. Referring to TABLE 2, the limit on the Hub-to-tip ratio is enforced, while the other restrictions are verified in the post-process. Additionally, the diffuser inlet Mach number must not exceed 0.95, while the rotational speed is treated as a degree of freedom in the analysis. As a general observation, all fluids exhibit similar behaviour across different expansion ratios, numbers of stages, and mass flows.

In the case of a single-stage GE, increasing the pressure ratio penalizes efficiency due to the rise in the relative Mach number at the rotor outlet, which violates the imposed limit ($M_{rel,out} < 1.4$) under expansion ratio conditions of 10 for all mass flow conditions. Indeed, in a single-stage turbine, the enthalpy drop cannot be distributed across multiple stages. Consequently, at significant β, the relative flow acceleration is substantial, resulting in supersonic Mach numbers. This penalty is expressed by the Kacker-Okapuu loss model [18], wherein the profile loss formula is determined by the $M_{rel,out}$ across various contributions. Specifically, the profile loss incorporates a factor that encompasses losses associated with supersonic flows at the blade trailing edge, along with an additional term that addresses relatively weak shock waves that may occur at the leading edge of a cascade due to flow acceleration. Moreover, in one stage GE, the strong stream acceleration leads to a tip peripheral speed closed to the imposed limit ($u_{tip} < 400$ m/s).

The degree of reaction is around 0.48 and 0.52 at the mean line guaranteeing a $\Lambda > 0$ at hub radius for all the investigated cases. Looking to Figure 6, the efficiency ranges from 89% to 94.5% with a good agreement with the preliminary results obtained with Eq. (4) and Eq. (5) presented in Figure 5, where the only mismatch in the trend (the η_{is} rise with the β increase) occurs with single stage GE.

Therefore, a detailed examination into the geometry is necessary to evaluate the design feasibility of the axial GE. These machineries show a compact design with a blade height for the rotor from 10 to 60 mm and a tip radius from 30 to 350 mm: H_2 GE are characterized by larger dimensions due to the higher volumetric flow. Turbomachinery that are characterized by small dimensions are not uncommon and they can be found in power cycle too. As described by Salah et al. [30], a 100 kW carbon dioxide turbine can reach a blade height up to 1.5-2 mm and a diameter up to 80-100 mm, depending on different boundary conditions. For instance, few examples of small turbine are presented in Organic Rankine Cycle.

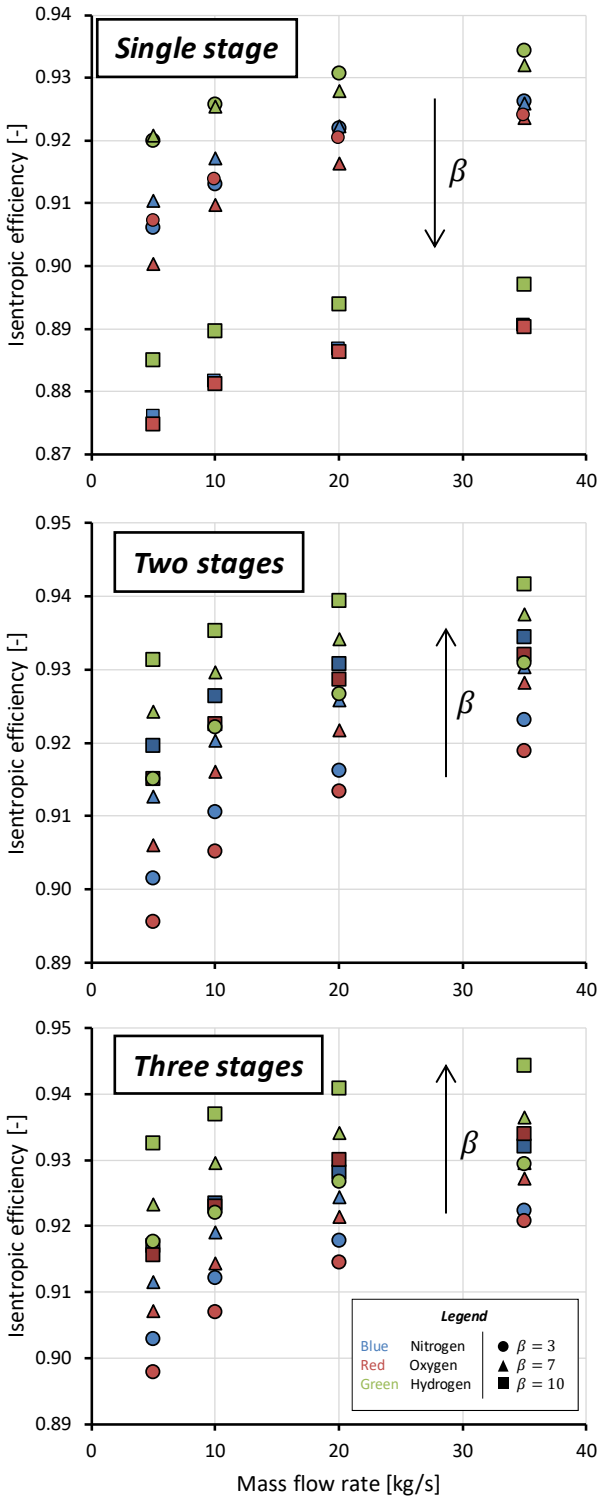

FIGURE 6: ISENTROPIC EFFICIENCY FOR THE AXIAL GE. UPPER: ONE STAGE, MIDDLE: TWO STAGES, LOWER: THREE STAGES.

Macchi and Astolfi [31] reported a rotor diameter for axial turbine up to 80 mm for $V_{r,is}$ from 1.2 to 20 at optimum specific speed and SP equal to 0.05 m. The authors presented also a 500 kW R125 and Hexane turbines with a diameter of 80 mm and 180 mm with an SP comparable with the investigated cases in this work [31]. On the contrary, in an N_2 closed Brayton cycle proposed by Park et al. [32], the two stages turbine has a maximum diameter of 2100 mm (mass flow of 4956 kg/s and mechanical power of 636 MW). Implementing innovative manufacturing processes to construct small machinery presents a challenge. However, it's notable that the recommended pipeline diameter, as per EIGA guidelines (which propose a velocity of 7 m/s in the range of 40-60 bar), ranges from 100 to 400 mm, aligning well with the dimensions of the gas expander.

The three stage design of the GE may be deemed suitable for N_2 and O_2 applications, whereas the H_2 GE demonstrates a u_{tip} exceeding the imposed limit. Regarding the increase of the stages number, it is possible to notice in Figure 7 (H_2 GE with a mass flow rate of 35 kg/s) that the u_{tip} of the last rotor, decreases and reaches a peripheral speed below the imposed limit where the total stages number is between 12 and 22 depending on pressure ratio while the η_{is} remains in the range presented in Figure 6.

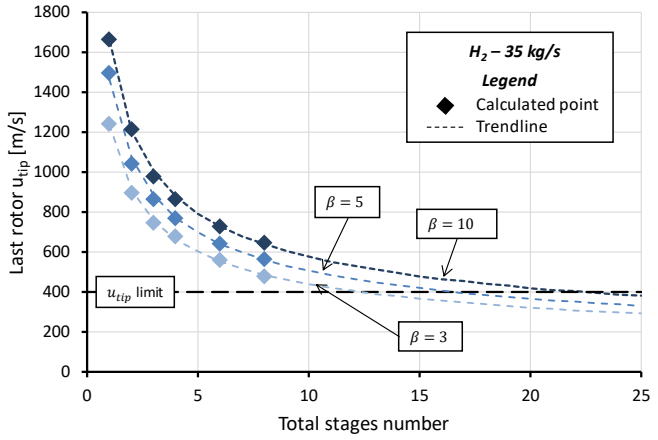

FIGURE 7: TREND OF THE LAST ROTOR U_{TIP} BY INCREASING THE TOTAL STAGES NUMBER FOR HYDROGEN WITH A MASS FLOW RATE OF 35 KG/S.

Similar results on stages number can be found also in the works of Hudson [33] and No et al [34]. Hudson investigated a H_2 turbine for space power system resulting an expander with 14 stage at β equal to 5, while No et al proposed a turbine in nuclear reactor adopting helium (a gas comparable with H_2) with 6 stages at β equal to 1.87. Besides the fact that the inlet expander condition and mass flow in [33] and [34] are different comparing the ones in this work, it is important to observe that when high w_{is} occurs is necessary to increase the number of stages as happens for steam turbine.

3.4 Case studies

In this section, the results concerning the case studies are presented. In *Case 1* (Figure 8), adopting the code AxialOpt, a maximum in the efficiency is obtained at 3 stages with a η_{is} equal to 93.1% leading to a generated power of 2425 kW, an EOT of -99.4°C and a thermal request for gas heating of 848.1 kW. Since the mass flow rate is significant (23.9 kg/s) the rotor blade height range from 1.4 cm in the first rotor to 2.4 cm in the third one, while the tip radius is 12.7 cm at GE outlet. Rotational speed is attested at 18.42 kRPM keeping however the tip peripheral speed (244.5 m/s at last stage) and the relative Mach number below the imposed limits. In *Case 2*, the maximum isentropic efficiency is found at 93.09% with a three stage GE, resulting into a power production of 1615.5 kW, a thermal demand of 461.3 kW and an EOT of -99.77°C. Three stage allows to have a relative Mach number in the order of 0.6 and 0.9, while the tip peripheral speed is 236 m/s in the first rotor and 244 m/s in the third one. Rotational speed is attested at 17.77 kRPM and the dimensions are still compact: the maximum radius tip is 13.1 cm, while the blade height is 23 mm.

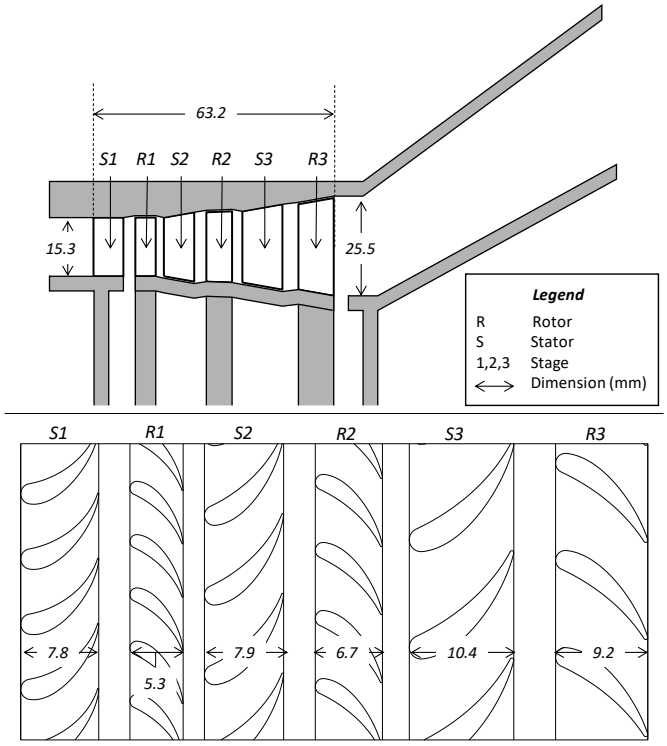

FIGURE 8: EXAMPLE OF GE (CASE 1). SECTION OF THE GAS EXPANDER (UPPER) AND BLADES PROFILES AT MEAN LINE (LOWER). DIMENSION IN MM.

The pressure ratio equal to 2, in *Case 3*, suggests the use of a single stage GE and that leads to an isentropic efficiency of 89.91%. The generated power is 523.3 kW and, since the gas is not preheated, the EOT has a value of -25.71°C. The rotational speed is 34.99 kPRM, but the rotor height blade is rather small (13.5 mm), while the tip radius is 5.3 cm leading to un tip

peripheral speed of 242 m/s. The low mass flow rate, in *Case 4*, suggests the unfeasibility of axial turbine, since the tip radius will be below 6 cm and leading to difficulties on the manufacturing: so radial GE are implemented. The $V_{r,is}$ is 5.03 for nitrogen and 4.92 for hydrogen, while the size parameter is 0.015 m for N_2 and 0.013 m H_2. According to the map in Figure 5, the isentropic efficiency for both GEs is roughly 83% leading to a generated power of 88.8 kW for nitrogen and 287.5 kW for hydrogen while the thermal demand for gas heating is 27.7 kW and 81 kW respectively. Table 6 summarizes the annual energy production, avoided emissions and the preliminary LCOE that ranges from 16 to 37 $/MWh.

TABLE 6: ANNUAL ELECTRIC ENERGY, AVOIDED EMISSION AND LCOE FOR EACH CASE.

Case	1	2	3	4
GE efficiency, %	93.1	93.09	89.9	83 (both GE)
Heat demand, kW	848	461.2	0	107.8 (total)
Energy, MWh/y	19116	12737	4126	2267 (total)
Avoided emission $tCO_{2,eq}$/y	1062	708	229	165 (total)
LCOE, $/MWh	16	22	37	18 (average)

Checking over the costs (Figure 9), GE accounts for 56 to 93% of the total equipment cost while the share of the heat exchanger does not exceed the 4% and the costs of generator and gearbox are direct consequence of the generated power.

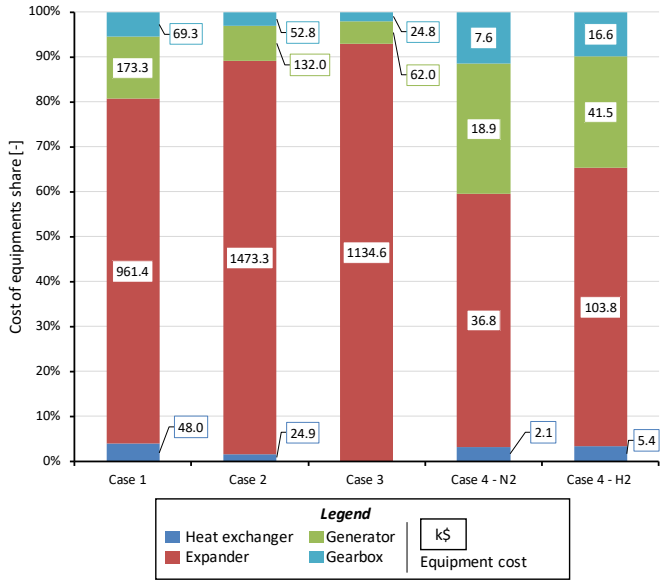

FIGURE 9: SHARE OF THE COST OF EQUIPMENT. LABEL INDICATES THE BARE COST IN K$. FOR CASE 3, THE HEAT EXCHANGER IS ABSENT.

Comparing to the produced power, the GE in *Case 3* is rather high. The first term in the expander correlation (Table 4) is a function of the gross power and represents a constant cost that is independent of the axial and radial dimensions, while the second term accounts for all the expenses of the stages design and manufacturing. Considering the GE inlet conditions, the specific power is approximately 46.5 kJ/kg leading to a size parameter equal to 1.73 m and so increases the bare cost of the component. On the other hand, in *Case 3* and *Case 4* the effect of SP is less evident (0.08 m versus 0.49 m), but the higher power generated in *Case 3* leads to a lower GE cost. Finally in *Case 4* the low SP and generated power grants a bare cost of 36.8 k$ for the nitrogen expander and 103.8 k$ for the hydrogen one. According to the data presented by the International Renewable Energy Agency [35], the LCOE for offshore wind is 80 $/MWh, 50 $/MWh for photovoltaic solar and 70 $/MWh for geothermal. The obtained LCOE is competitive with conventional renewable energy sources and common power cycles, thanks to the reduced plant complexity. These cases, drawn from both literature and industry, demonstrate scenarios where industrial GE can be adopted under various boundary conditions. However, they also emphasize the necessity for a case-by-case design approach.

3.5 Discussion on practical issue

Following the previous discussion, three different concerns can be identified for the GE implementation in real industrial environment: i) EOT < 0°C, ii) material compatibility at EOT < 0°C and iii) safety issues.

The first issue addressed is the presence of iced particles in the stream post-expansion, particularly when the EOT falls below 0°C. In the NG distribution network, regulations such as the Italian UNI 9167 mandate an EOT above 5°C to prevent methane hydrate formation [19]. Therefore, preheating the stream becomes necessary to prevent such issues, albeit at the expense of consuming more natural gas. While this method could potentially increase turbomachinery work due to higher EIT the investigated gases, known for their high purity (up to 99.9999%), shouldn't typically form iced particles. Moreover, the boiling temperature is lower than the isentropic EOT discussed, ensuring no fluid condensation. In industrial applications is common the presence of a low-medium heat recovery source (above 100°C) could facilitate preheating. Even if EOT falls below 0°C, it's crucial to note that the POD doesn't necessarily coincide with the POU (Figure 1). Thus, cryogenic gas presence in the industrial process can be avoided, with any ice formation occurring externally around the tubes. Restoring ambient temperature can be easily achieved through pipeline natural convection.

TABLE 7: SUMMARY OF THE DISCUSSION ON PRACTICAL ISSUE

Gas	Safety issue	Recommended GE metal
N_2	Simple asphyxiant	Stainless steel (i.e. 316)
O_2	Combustion agent	Nickel-based alloys
H_2	Fuel	Carbon steel

Ensuring safety in operations with an expected EOT below 0°C requires careful material selection to prevent centrifugal stress. In power generation, stainless steels are commonly used for low-temperature applications, while Inconel is preferred for high-temperature ones [36]. This discussion highlights the importance of matching fluids with metals, particularly focusing on O_2 and H_2 due to their high risk. Hurlich's work [37] illustrates the low-temperature resistance of various metals (Figure 10), with Table 7 summarizes the analysis.

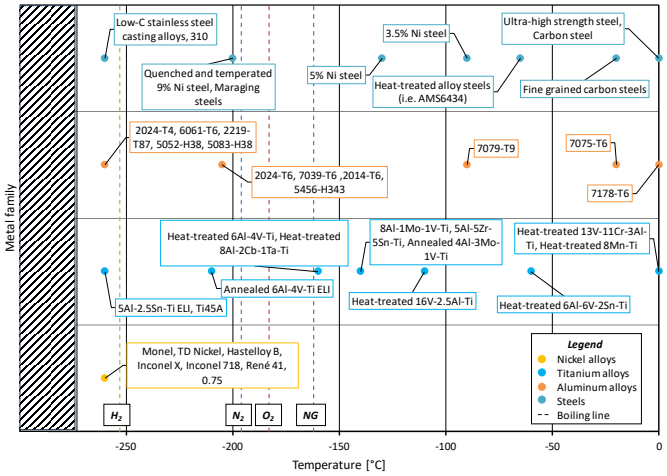

FIGURE 10: MATERIALS RESISTANT TO EXTREMELY LOW TEMPERATURES. DATA RETRIVED FROM [37].

Nitrogen, often considered harmless because it's nontoxic and inert, can actually pose a risk by displacing oxygen, causing asphyxiation. According to a survey by the German Aerospace Centre [38] nitrogen can be safely used with stainless and ferritic steel, aluminium and copper.

Ensuring safety in high-pressure oxygen systems is crucial due to the reactive nature of oxygen. Materials that are inert in regular atmospheres can combust violently in oxygen, leading to a higher accident rate. Metals are selected based on their ignition susceptibility, often relying on a protective oxide coating. Nickel alloys, especially pure nickel and nickel-based alloys like Inconel 718, are considered excellent choices for combustion support at high pressures [39]. Monel alloys, such as Monel 400 and K-500, are recognized as the least ignitable, even at high oxygen pressures. Certain Hastelloy alloys, like C-22 and C-276, exhibit higher ignition resistance than stainless steels and Inconel 718 [39]. Stainless steels are widely used due to their superior ignition and burn resistance compared to titanium and aluminium alloys. Burn-resistant metallic alloys are chosen based on recommendations from associations like the Compressed Gas Association and EIGA [40] [41]. Nickel-based alloys, known for their heightened burn resistance, have an exemption pressure approximately six times higher than stainless steels [42]. Despite this, stainless steels remain preferred for oxygen service pipelines in various industries due to their favourable properties, availability, manufacturability, corrosion resistance, shorter lead times, and cost-effectiveness [43]. Nickel-based alloys, however, could be considered for expander manufacturing due to the considerable gas velocity through them.

The challenges posed by hydrogen exposure in equipment arise from its absorption and permeation through metals. The Technical Reference for Hydrogen Compatibility of Materials [44] provides insights into material considerations but lacks specific guidance on material selection based on operating conditions. The focus in this context is on the proposed H_2 GE, operating from slightly above ambient to cryogenic temperatures. Hydrogen embrittlement, resulting in decreased ductility despite unaltered strength, is a significant concern. Campari et al. [45] reveal temperature dependence in hydrogen-induced crack propagation, with austenitic stainless steels exhibiting maximum embrittlement susceptibility between 70 and 20°C. Other works indicate that the risk of hydrogen stress cracking in steels is highest around 20°C [45], decreasing with rising temperatures, and has a peak around -100°C for certain alloys [46]. High-Manganese steel demonstrates enhanced resistance in the -150 to 25°C range, aligning with the proposed GE temperature range. High-strength materials, like Alloy Inconel 625, show superior resistance to hydrogen compared to others [47]. Titanium alloys, suitable for rotating parts, may be susceptible to hydrogen embrittlement, with beta alloys showing more resistance [48]. For hydrogen compressor components, recommended materials include carbon steel, UNS G43400 for shafts, and UNS S17400 or UNS S15500 for impellers. Standard abradable or rub-tolerant seal materials like mica-filled PTFE, PEEK, or PAI are suggested for shaft seals [49]. The same considerations about hydrogen compressors could be extended also for the hydrogen expanders as intended in this work.

4. CONCLUSION

In this paper, the potential for energy recovery in industrial gas distribution networks is proposed. The replacement of the expansion valve with a gas expander emerges as a viable solution, particularly in energy-intensive industrial sectors such as steel and glass production. The gas expander can ensure an isentropic efficiency ranging from 85% to 94%, depending on machinery design, mass flow rate, and thermodynamic operating conditions. Application of this technology in real-world scenarios demonstrates an intriguing solution with low cost and environmental impact. Furthermore, with careful system design, it is possible to address issues related to material compatibility and safety precautions. However, a potential bottleneck for this application lies in the limited availability of data concerning the extension of the distribution network, as well as characteristics and final utilizations. Therefore, while technical analysis demonstrates the feasibility of this solution, a more detailed market analysis will aid in the widespread adoption of this promising technology.

ACKNOWLEDGEMENTS

This publication was produced while attending the PhD program in PhD in Sustainable Development and Climate Change (www.phd-sdc.it) at the IUSS Pavia, Cycle XXXVIII,

with the support of a scholarship financed by the Ministerial Decree no. 351 of 9th April 2022, based on the NRRP - funded by the European Union – Next Generation EU.

REFERENCES

[1] S. M. Ebrahimi Saryazdi, F. Rezaei, and Y. Saboohi, "Optimal detailed design and performance assessment of natural gas pressure reduction stations system equipped with variable inlet guide vane radial turbo-expander for energy recovery," *J. Nat. Gas Sci. Eng.*, vol. 96, p. 104222, Dec. 2021, doi: 10.1016/J.JNGSE.2021.104222.

[2] A. Zabihi and M. Taghizadeh, "Feasibility study on energy recovery at Sari-Akand city gate station using turboexpander," *J. Nat. Gas Sci. Eng.*, vol. 35, pp. 152–159, Sep. 2016, doi: 10.1016/J.JNGSE.2016.08.054.

[3] "Prodotti | SIAD Macchine Impianti." https://www.siadmi.com/it/prodotti (accessed Oct. 17, 2023).

[4] "Facts & Figures - EIGA : European Industrial Gases Association." https://www.eiga.eu/the-industry/statistics/ (accessed Nov. 01, 2023).

[5] "Air separation plants | Linde Engineering." https://www.linde-engineering.com/en/process-plants/air-separation-plants/index.html (accessed Oct. 17, 2023).

[6] "Hydrogen and synthesis gas plants | Linde Engineering." https://www.linde-engineering.com/en/process-plants/hydrogen_and_synthesis_gas_plants/index.html (accessed Oct. 17, 2023).

[7] "The European Hydrogen Backbone (EHB) initiative | EHB European Hydrogen Backbone." https://ehb.eu/ (accessed Dec. 21, 2023).

[8] F. Kong *et al.*, "A novel nitrogen pipeline system for recycling pressure energy: System model and energy efficiency economic analysis," *Appl. Therm. Eng.*, vol. 219, p. 119475, Jan. 2023, doi: 10.1016/J.APPLTHERMALENG.2022.119475.

[9] S. Bucsa *et al.*, "Exergetic Analysis of a Cryogenic Air Separation Unit," *Entropy 2022, Vol. 24, Page 272*, vol. 24, no. 2, p. 272, Feb. 2022, doi: 10.3390/E24020272.

[10] D. R. Vinson, "Air separation control technology," *Comput. Chem. Eng.*, vol. 30, no. 10–12, pp. 1436–1446, Sep. 2006, doi: 10.1016/J.COMPCHEMENG.2006.05.038.

[11] J. Zhang, H. Meerman, R. Benders, and A. Faaij, "Technical and economic optimization of expander-based small-scale natural gas liquefaction processes with absorption precooling cycle," *Energy*, vol. 191, p. 116592, Jan. 2020, doi: 10.1016/J.ENERGY.2019.116592.

[12] G. Subbaraman, "Final Report-Rev0 Emerging and Existing Oxygen Production Technology Scan and Evaluation," 2018, Accessed: Dec. 21, 2023. [Online]. Available: www.gastechnology.org

[13] M. Papapetrou, G. Kosmadakis, A. Cipollina, U. La Commare, and G. Micale, "Industrial waste heat: Estimation of the technically available resource in the EU per industrial sector, temperature level and country," *Appl. Therm. Eng.*, vol. 138, pp. 207–216, Jun. 2018, doi: 10.1016/J.APPLTHERMALENG.2018.04.043.

[14] "Aspen Plus | Leading Process Simulation Software | AspenTech." https://www.aspentech.com/en/products/engineering/aspen-plus (accessed Apr. 11, 2023).

[15] E. W. Lemmon, I. H. Bell, M. L. Huber, and M. O. Mclinden, "REFPROP Documentation Release 10.0," 2018.

[16] A. Perdichizzi and G. Lozza, "Design Criteria and Efficiency Prediction for Radial Inflow Turbines," *Proc. ASME Turbo Expo*, vol. 1, Mar. 2015, doi: 10.1115/87-GT-231.

[17] M. Gambini and M. Vellini, "Turbomachinery," 2021, doi: 10.1007/978-3-030-51299-6.

[18] R. Agromayor and L. O. Nord, "Preliminary Design and Optimization of Axial Turbines Accounting for Diffuser Performance," *Int. J. Turbomachinery, Propuls. Power 2019, Vol. 4, Page 32*, vol. 4, no. 3, p. 32, Sep. 2019, doi: 10.3390/IJTPP4030032.

[19] "UNI 9167-1:2020 - UNI Ente Italiano di Normazione." https://store.uni.com/uni-9167-1-2020 (accessed Nov. 26, 2023).

[20] R. E. Macchi, "On the Influence of the Number of Stages on the Efficiency of Axial-. Lozza Flow Turbines," 1982. [Online]. Available: http://asmedigitalcollection.asme.org/GT/proceedings-pdf/GT1982/79566/V001T01A016/2394006/v001t01a016-82-gt-43.pdf

[21] "FGC Group LLC - Consulting & Engineering | Products | Float Glass Industry." https://www.fgcgroupllc.com/float_glass_plant.html (accessed Nov. 29, 2023).

[22] A. Arasto, E. Tsupari, J. Kärki, J. Lilja, and M. Sihvonen, "Oxygen blast furnace with CO2 capture and storage at an integrated steel mill—Part I: Technical concept analysis," *Int. J. Greenh. Gas Control*, vol. 30, pp. 140–147, Nov. 2014, doi: 10.1016/J.IJGGC.2014.09.004.

[23] "Servizi On-line alla cittadinanza e alle imprese." https://inlinea.cittametropolitana.mi.it/files/aia/R.G. 5936_2018_Vetrobalsamo_atto completo.pdf

[24] "Comparison of Gear Efficiencies - Spur, Helical, Bevel, Worm, Hypoid, Cycloid." https://www.meadinfo.org/2008/11/gear-efficiency-spur-helical-bevel-worm.html (accessed Dec. 07, 2023).

[25] "Greenhouse gas emission intensity of electricity generation in Europe." https://www.eea.europa.eu/en/analysis/indicators/greenhouse-gas-emission-intensity-of-1 (accessed Nov. 03, 2023).

[26] E. Macchi Co-Supervisor, I. Matteo Carmelo Romano

Ing Paola Bombarda Tutor, S. Campanari Coordinator, and C. Enrico Bottani candidate Marco Astolfi XXVI ciclo, “POLITECNICO DI MILANO An Innovative Approach for the Techno-Economic Optimization of Organic Rankine Cycles”.

[27] M. Astolfi, M. C. Romano, P. Bombarda, and E. Macchi, “Binary ORC (Organic Rankine Cycles) power plants for the exploitation of medium–low temperature geothermal sources – Part B: Techno-economic optimization,” *Energy*, vol. 66, pp. 435–446, Mar. 2014, doi: 10.1016/J.ENERGY.2013.11.057.

[28] R. Ghanaee and A. A. Foroud, “Economic analysis and optimal capacity sizing of turbo-expander-based microgrid,” *IET Renew. Power Gener.*, vol. 11, no. 4, pp. 511–520, Mar. 2017, doi: 10.1049/IET-RPG.2016.0390.

[29] “Cost Indices – Towering Skills.” https://toweringskills.com/financial-analysis/cost-indices/ (accessed Dec. 26, 2023).

[30] S. I. Salah *et al.*, “Mean-Line Design of a Supercritical CO2 Micro Axial Turbine,” *Appl. Sci. 2020, Vol. 10, Page 5069*, vol. 10, no. 15, p. 5069, Jul. 2020, doi: 10.3390/APP10155069.

[31] E. Macchi and M. Astolfi, *Organic Rankine Cycle (ORC) Power Systems - 1st Edition*, 1st Editio. 2017. doi: https://doi.org/10.1016/C2014-0-04239-6.

[32] J. H. Park, J. Yoon, J. Eoh, H. Kim, and M. H. Kim, “Optimization and sensitivity analysis of the nitrogen Brayton cycle as a power conversion system for a sodium-cooled fast reactor,” *Nucl. Eng. Des.*, vol. 340, pp. 325–334, Dec. 2018, doi: 10.1016/J.NUCENGDES.2018.09.037.

[33] “Hydrogen turbines for space power systems: A simplified axial flow gas turbine model (Conference) | OSTI.GOV.” https://www.osti.gov/biblio/5226975 (accessed Dec. 30, 2023).

[34] H. Cheon No, J. H. Kim, and H. M. Kim, “A REVIEW OF HELIUM GAS TURBINE TECHNOLOGY FOR HIGH-TEMPERATURE GAS-COOLED REACTORS,” *Nucl. Eng. Technol.*, vol. 39, no. 1, 2007.

[35] IRNEA, “IRENA (2022), Renewable Power Generation Costs in 2021, International Renewable Energy Agency, Abu Dhabi. ISBN 978-92-9260-452-3,” *Int. Renew. Energy Agency*, p. 160, 2022, Accessed: Oct. 18, 2023. [Online]. Available: https://www.irena.org/-/media/Files/IRENA/Agency/Publication/2018/Jan/IRENA_2017_Power_Costs_2018.pdf

[36] G. K. Salwan, R. Subbarao, and S. Mondal, “Comparison and selection of suitable materials applicable for gas turbine blades”, doi: 10.1016/j.matpr.2021.05.003.

[37] A. Hurlich, “Low temperature metals,” *Conf.Proc.C*, vol. 680610, pp. 311–325, 1968, Accessed: Jan. 03, 2024. [Online]. Available: https://wpw.bnl.gov/rgupta/wp-content/uploads/sites/9/2023/02/1968-summer-study.pdf

[38] R. Lechler, “Final Report-Revised Version-"Literature Survey of Materials compatible with Propellants" Additive Manufacturing Based Bellows Working Package 1: Selection of a suitable Material and Process Combination Final Report: Literature Survey of Materials compatible with Propellants,” 2015.

[39] “Safety Standard for Oxygen and Oxygen Systems: Guidelines for Oxygen System Design, Materials Selection, Operations, Storage, and Transportation.” 1996.

[40] “CGA’s G-4.4 Publication Guides the Safe Design, Operation, and Maintenance of Oxygen Pipeline and Piping Systems - Compressed Gas Association.” https://www.cganet.com/cga-g-4-4-publication-guides-safe-design-operation-oxygen-pipeline-and-piping-systems/ (accessed Dec. 30, 2023).

[41] Eiga, “FIRE HAZARDS OF OXYGEN AND OXYGEN-ENRICHED ATMOSPHERES”, Accessed: Dec. 30, 2023. [Online]. Available: www.eiga.eu

[42] V. C. Shunmugasamy, G. J. A. Chiffoleau, E. Forsyth, N. J. Laycock, A. Kruijer, and B. Mansoor, “On the metals compatibility assessment for oxygen service,” *J. Loss Prev. Process Ind.*, vol. 74, p. 104670, Jan. 2022, doi: 10.1016/J.JLP.2021.104670.

[43] Eiga, “OXYGEN PIPELINE AND PIPING SYSTEMS Doc 13/20”, Accessed: Dec. 30, 2023. [Online]. Available: https://www.eiga.eu/uploads/documents/DOC013.pdf

[44] C. W. San Marchi and B. P. Somerday, “Technical reference for hydrogen compatibility of materials.,” Sep. 2012, doi: 10.2172/1055634.

[45] A. Campari, F. Ustolin, A. Alvaro, and N. Paltrinieri, “A review on hydrogen embrittlement and risk-based inspection of hydrogen technologies,” *Int. J. Hydrogen Energy*, vol. 48, no. 90, pp. 35316–35346, Nov. 2023, doi: 10.1016/J.IJHYDENE.2023.05.293.

[46] K. O. Bae, T. T. Nguyen, J. Park, J. S. Park, and U. B. Baek, “Temperature dependency of hydrogen-related impact energy degradation of type 304 austenitic stainless steel,” *J. Mech. Sci. Technol.*, vol. 37, no. 6, pp. 2891–2901, Jun. 2023, doi: 10.1007/S12206-023-0515-5/METRICS.

[47] P. D. Hicks and C. J. Altstetter, “Internal hydrogen effects on tensile properties of iron- and nickel-base superalloys,” *Metall. Trans. A*, vol. 21, no. 1, pp. 365–372, Jan. 1990, doi: 10.1007/BF02782416/METRICS.

[48] H. Heshmat, “Oil-free centrifugal hydrogen compression technology demonstration,” May 2014, doi: 10.2172/1225266.

[49] “The world turns to Elliott. Materials for Hydrogen Compression”, Accessed: Dec. 30, 2023. [Online]. Available: https://netl.doe.gov/sites/default/files/netl-file/21TMCES_Bauer.pdf